A Cloud Climatology of the Southern Great Plains ARM CART

STEVEN M. LAZARUS, STEVEN K. KRUEGER, AND GERALD G. MACE

Department of Meteorology, University of Utah, Salt Lake City, Utah

(Manuscript received 14 January 1999, in final form 2 August 1999)

ABSTRACT

Cloud amount statistics from three different sources were processed and compared. Surface observations from a National Centers for Environmental Prediction dataset were used. The data (Edited Cloud Report; ECR) consist of synoptic weather reports that have been edited to facilitate cloud analysis. Two stations near the Southern Great Plains (SGP) Cloud and Radiation Test Bed (CART) in north-central Oklahoma (Oklahoma City, Oklahoma and Wichita, Kansas) were selected. The ECR data span a 10-yr period from December 1981 to November 1991. The International Satellite Cloud Climatology Project (ISCCP) provided cloud amounts over the SGP CART for an 8-yr period (1983–91). Cloud amounts were also obtained from Micro Pulse Lidar (MPL) and Belfort Ceilometer (BLC) cloud-base height measurements made at the SGP CART over a 1-yr period. The annual and diurnal cycles of cloud amount as a function of cloud height and type were analyzed. The three datasets closely agree for total cloud amount. Good agreement was found in the ECR and MPL–BLC monthly low cloud amounts. With the exception of summer and midday in other seasons, the ISCCP low cloud amount estimates are generally 5%–10% less than the others. The ECR high cloud amount estimates are typically 10%–15% greater than those obtained from either the ISCCP or MPL–BLC datasets. The observed diurnal variations of altocumulus support the authors' model results of radiatively induced circulations.

1. Introduction

Cloud amount is the most basic measure of cloudiness. Because clouds are a major component of the climate system, it is important to have quality cloud observations. This includes, but is not limited to, knowledge of quantities such as the average cloud amount as a function of cloud type, season, and time of day. Clouds remain a source of uncertainty in climate models. Fluctuations in outgoing longwave radiation have been linked to temporal and spatial variations of cloud amount (Short and Wallace 1980) and the mechanisms that couple the large-scale dynamics with cloud-scale convection are not well understood. Furthermore, diurnal and annual variations of cloud amount are dependent on the geographical location (Allis and Raman 1995). Thus, if we are to fully understand the interaction between clouds and the earth's climate we need to examine cloud cover on scales that can resolve this variability. Cloud statistics, especially those over the continent that often show pronounced diurnal cycles, can be utilized to evaluate general circulation models (GCMs), which employ simplified representations of subgrid-scale processes.

The Atmospheric Radiation and Measurements program (ARM; Stokes and Schwartz 1994) Southern Great Plains (SGP) Cloud and Radiation Test Bed (CART) is host to a bevy of radiometric and cloud-observing instruments dedicated toward assisting ARM in reaching its objective to develop/improve cloud and radiative parameterizations for use in GCMs. If cloud observations collected at the SGP ARM CART are to be used to evaluate GCM performance or to develop new cloud parameterization schemes, some measure of the degree of reliability and representativeness of these observations must be obtained. Data quality can be assessed by comparing cloud observations from a variety of measurement platforms. Direct comparisons are difficult due to differences in perspective or view as well as the different temporal and spatial scales of the observations.

The most comprehensive cloud climatologies have been composited from a variety of observation types (e.g., Newell et al. 1970). For example, data collected from satellites are a natural complement to those obtained by a surface observer as the former (latter) yields relatively accurate estimates of high (low) cloud amounts. In addition to these sources, another potential contributor to a CART climatology is the millimeter-wavelength cloud radar (MMCR; Moran et al. 1998), which has the capability to provide cloud information through the entire troposphere. However, the operation of the MMCR has been of too short duration to, as of yet, contribute to a climatology. Surface-based remote sensors such as the Micro Pulse Lidar (MPL; Spinhirne

Corresponding author address: Dr. Steven Lazarus, Department of Meteorology, University of Utah, Salt Lake City, UT 84112-0110.
E-mail: slazarus@atmos.met.utah.edu

1993) and the Belfort Laser Ceilometer (BLC), however, have operated side-by-side since 1993 at the SGP ARM CART. The MPL and BLC accurately detect the occurrence and base height of cloud in the vertical column directly above the instruments. Herein we present a regional cloud climatology of the SGP ARM CART produced from three independent sources: human, satellite, and surface-based remote sensor observations. These sources and their characteristics are described in section 2. In section 3a we present an intercomparison of the three platforms, while in sections 3b and 3c the statistics of low, middle, high, and total clouds (for all three sources) are presented. In section 3d, we present some additional results classified by cloud type derived from synoptic reports only.

2. Datasets

a. Synoptic cloud reports

Although nighttime observations of cloudiness made by meteorologists are sometimes questionable and estimates of total cloud amount are typically high (Hughes 1984), the human eye is still the most reliable source of *cloud type* data. Human observations are a long-standing source of global and regional cloud climatologies. They remain one of the best resources for verification of cloud statistics generated by GCMs. We use a cloud observation dataset from Hahn et al. (1996) developed from synoptic (i.e., human) weather reports over the globe for the 10-yr period from December 1981 to November 1991. This period was chosen to correspond with the International Satellite Cloud Climatology Project (ISCCP; Rossow and Schiffer 1991). The land station reports (a National Centers for Environmental Prediction dataset), were obtained from the National Center for Atmospheric Research and contain approximately 144 million 6-hourly reports. The dataset was constructed to facilitate the analysis of cloud observations by removing or correcting inconsistent and erroneous reports, and by including only information from the synoptic weather reports pertaining directly to clouds. Corrections are encoded in each Edited Cloud Report (ECR) such that the original report can be reconstructed.

While the amount of low-level cloud is specified directly in the synoptic code, upper-level cloud amount is often obscured. However, under certain conditions a quantity referred to as the ''amount-when-present'' (AWP) can be estimated at all levels. The AWP is defined as the average fraction of the sky that is covered by a particular cloud type when it is present. For low clouds, the AWP is simply the low cloud amount. Upper-level AWP can be estimated (whether visible or not) by utilizing the random overlap assumption (ROL); that is,

$$(1 - A_T) = (1 - A_L)(1 - A_U), \qquad (1)$$

where A_T and A_L are the fractional amounts (ranging from 0 to 1) of total and low-level cloud visible from below (both of which are given in the synoptic report), and A_U is the upper-level ROL AWP. Note that A_L can represent low or midlevel clouds [see Table 1 for the World Meteorological Organisation (WMO) cloud classification scheme] while A_U refers to midlevel or high-level clouds. Although Eq. (1) can be applied to individual observations, it is valid (at best) only in a statistical sense; that is, it is correct only if the ROL is valid and averaged over many observations. Equation (1) relates the clear-sky fraction (i.e., the fraction of the celestial dome that is free of clouds) to the product of the clear-sky fractions of the layers (i.e., the fraction of the celestial dome that is free of clouds at each particular level). Using Eq. (1), Hahn et al. estimate the upper-level cloud amount A_U in the presence of an underlying cloud layer. In the absence of a low cloud layer, the amount of middle cloud can be obtained directly from the synoptic report and when both low and middle cloud is absent, the amount of high cloud is given by the report. If clouds are present at all three levels simultaneously, Eq. (1) contains two unknowns and cannot be solved. Hahn et al. note that estimates of A_U become inaccurate for large values of A_L and restrict calculations of upper level AWP to values of A_L less than 7/8. However, it should be noted that this ($A_L \neq 7/8$) is not necessary because estimates of A_U using the ROL are predicated on many realizations. The accuracy of Eq. (1) will depend on the actual cloud distribution (Tian and Curry 1989). Two additional cloud overlap assumptions are maximum and minimum overlap. Tian and Curry showed that the maximum overlap assumption best described situations in which there are two adjacent cloud layers (i.e., two cloud layers that are not separated by a clear layer) while the random overlap assumption is best for cases where there were discrete cloud layers (two cloud layers separated by a clear layer).

TABLE 1. Cloud types.

Genera	Level
Cumulus, stratocumulus, stratus, cumulonimbus	Low
Altocumulus, altostratus, nimbostratus	Middle
Cirrus, cirrocumulus, cirrostratus	High

Other cloud climatology statistics include the *cloud occurrence frequency* COF (fraction of observations in which a particular cloud type is present whether visible from the surface or not) and cloud fraction or cloud amount (the visible fraction of sky covered by that cloud type). In practice, the COF is calculated by dividing the number of times a particular cloud type is observed by the number of synoptic cloud reports that contained information about that cloud type. Similar to Hahn et al., we choose a method to estimate cloud cover (the fraction of the sky covered by a particular cloud type) that attempts to determine, as closely as possible, the actual amount (i.e., the cloud fraction present whether visible or not) instead of the nonoverlapped amounts (the frac-

tion of a particular cloud type seen from below). With this in mind, we calculate the *time-averaged cloud amount* (TCA) for total, low, middle, and high clouds as well as for individual cloud types. Low, middle, and high cloud genera are defined by the WMO sky cover code (World Meteorological Organisation 1988) according to the cloud-base height (Table 1). The TCA, which is used to construct the ECR cloud climatology presented herein, can be computed by multiplying the COF by the AWP (Warren et al. 1988),

$$\mathrm{TCA}^{\mathrm{NOL}} = \mathrm{COF} \times \mathrm{AWP}^{\mathrm{NOL}}, \quad (2)$$

where NOL is the nonoverlapped cloud amount, that is, the cloud fraction visible from the surface. The $\mathrm{TCA}^{\mathrm{NOL}}$ is the time average of the NOL fractional cloud cover. One can calculate the $\mathrm{TCA}^{\mathrm{NOL}}$ directly by summing over the cloud amount visible (from below) for a particular cloud type (low, middle, or high) and dividing by the total number of observations (including clear-sky reports). This method is equivalent to using Eq. (2) directly. We then apply the ROL Eq. (1) to the NOL ECR TCAs. For three cloud layers, the total TCA (as seen by a surface observer) can be expressed as

$$\mathrm{TCA}_T = \mathrm{TCA}_L^{\mathrm{NOL}} + \mathrm{TCA}_M^{\mathrm{NOL}} + \mathrm{TCA}_H^{\mathrm{NOL}}, \quad (3)$$

where the subscripts *T*, *L*, *M*, and *H* denote total, low, middle, and high clouds, respectively. The clear-sky fraction $(1 - \mathrm{TCA}_T)$ using the ROL; that is, Eq. (2) is

$$(1 - \mathrm{TCA}_T) = (1 - \mathrm{TCA}_L^{\mathrm{ROL}})(1 - \mathrm{TCA}_M^{\mathrm{ROL}})(1 - \mathrm{TCA}_H^{\mathrm{ROL}}). \quad (4)$$

Assuming there is no high cloud layer, we can solve Eq. (4) for $\mathrm{TCA}_M^{\mathrm{ROL}}$, and substituting Eq. (3) we obtain an expression relating the midlevel ROL TCAs with the ECR-observed midlevel NOL TCAs,

$$\mathrm{TCA}_M^{\mathrm{ROL}} = \frac{\mathrm{TCA}_M^{\mathrm{NOL}}}{1 - \mathrm{TCA}_L^{\mathrm{NOL}}}, \quad (5)$$

where we used $\mathrm{TCA}_L^{\mathrm{ROL}} = \mathrm{TCA}_L^{\mathrm{NOL}}$. If all three cloud layers are present, we solve Eq. (4) for $\mathrm{TCA}_H^{\mathrm{ROL}}$ by substituting Eq. (5) and $\mathrm{TCA}_L^{\mathrm{ROL}} = \mathrm{TCA}_L^{\mathrm{NOL}}$,

$$\mathrm{TCA}_H^{\mathrm{ROL}} = \frac{\mathrm{TCA}_H^{\mathrm{NOL}}}{1 - \mathrm{TCA}_L^{\mathrm{NOL}} - \mathrm{TCA}_M^{\mathrm{NOL}}}. \quad (6)$$

The ROL TCA is equal to the NOL TCA divided by the clear-sky fraction of the underlying layer(s). Equations (5) and (6) are used to construct the ECR climatology. As one might expect, $\mathrm{TCA}_H^{\mathrm{ROL}} \geq \mathrm{TCA}_H^{\mathrm{NOL}}$ and $\mathrm{TCA}_M^{\mathrm{ROL}} \geq \mathrm{TCA}_M^{\mathrm{NOL}}$.

Our method for estimating upper-level cloud amount [Eqs. (5) and (6)] differs from that of Hahn et al., who compute the amounts of upper-level cloud by separately computing the COF and AWP and then multiplying the results. They assume random overlap to estimate the AWP only and apply this to individual observations while our method assumes random overlap in the statistical mean sense. Comparison of their method with ours for idealized data (i.e., for a random specification of the NOL cloud amounts) indicates that estimates of the upper-level cloud amount do not differ significantly ($\leq$3%).

We combine ECR data from two reporting stations within the SGP CART site: Oklahoma City, Oklahoma (approximately 100 km to the south of the CART site), and Wichita, Kansas (approximately 100 km to the north of the CART site). The data for these two stations were sampled by month, season, and time of day (0000, 0600, 1200, and 1800 UTC). The UTC is shifted to local standard time by subtracting 6 h.

b. MPL and BLC

This dataset was created by combining cloud-base records from the Micro Pulse Lidar (MPL; Spinhirne 1993) and Belfort Laser Ceilometer (BLC) at the north-central Oklahoma ARM CART. Surface-based remote sensors such as the MPL and the BLC have operated side-by-side since 1993 at the ARM CART. In tandem, the two instruments generate a more complete record of cloud base than either does individually because the BLC yields better estimates of cloud-base occurrence in the lowest few kilometers than does the MPL due to short-range detection ambiguities of the MPL. The long-range detection, however, of the MPL is quite good—detecting tenuous cirrus to altitudes greater than 10 km, while MPL data are inspected for clouds up to 18 km. [The processing of MPL raw signal to determine cloud-base height is presented in more detail by Clothiaux et al. (1998).] Because the instruments have different sampling frequencies, the resulting datasets are combined in such a way as to correspond to the coarser temporal resolution of the MPL.

If the BLC did not observe clouds below 3 km, the MPL data were inspected for clouds above 3 km. Both the MPL and BLC accurately detect the occurrence and height of the lowest cloud in a vertical column directly above the instrument. As a result, cloud frequencies obtained from the MPL and BLC may vary substantially from the frequencies measured by an instrument that could sense clouds at all levels (e.g., MMCR) or from that of an observer with a full-sky view. *We assume that, for the MPL–BLC, the AWP is 1. Consequently, the COF is equivalent to the TCA.* We used cloud occurrence data (from more than one million observations) during the 12-month period beginning April 1994 to compile the joint MPL–BLC climatology. We binned these observations according to cloud-base height, time of day, and month. The $\mathrm{TCA}^{\mathrm{NOL}}$ was calculated by taking the number of reports for which a cloud type is observed and dividing by the total number of reports. The ROL TCAs were then calculated using Eqs. (5) and (6). Low, middle, and high cloud categories are delineated by the International Cloud Atlas cloud étage using the temperate classification [heights are above ground level (AGL)]:

Low cloud	0–2 km
Middle cloud	2–5 km
High cloud	5–13 km.

To avoid overlap with the high cloud étage, the middle étage is taken to extend to a height of 5 km only. Note that the above cloud classification is sufficiently broad so as to contain a statistically significant number of observations.

c. International Satellite Cloud Climatology Project

The ISCCP has collected radiance data from radiometers on weather satellites since 1983 (Rossow and Schiffer 1991). Part of this collection consists of the stage C cloud data products obtained from global analysis of the 0.6-μm visible (VIS) and 11-μm infrared (IR) radiances from as many as six satellites (Rossow and Walker 1991). Herein we use a subset of the stage C data referred to as stage C2. The C2 data, obtained from the NASA Langley Research Center, are monthly summaries of the C1 data. The C2 data are averaged over the month for individual times of day (0000, 0300, 0600, . . . UTC) to preserve information concerning the diurnal variability.

ISCCP cloud amount is determined from two quantities: the number of cloudy pixels and the total number of image pixels in the specified grid cell. (While the initial image pixel size is about 4–8 km, the C2 data have been sampled to a spacing of approximately 30 km. It is these subsampled data that serve as the input to the ISCCP cloud climatology presented herein.) Because of the bias associated with detecting nocturnal low-level clouds using IR radiances alone, the C2 data have been modified by the ISCCP such that nighttime estimates of *total* cloud amount are adjusted using the mean differences between the VIS–IR and IR only results measured during the daytime. The reader is referred to Rossow and Schiffer (1991) for a more complete description of the ISCCP cloud detection algorithm.

The C2 statistics were compiled from data on an equal area grid defined by a 2.5° latitude increment and a variable longitude increment. The C2 data were sampled over an 8-yr period from 1983 to 1991 for the grid cell containing the the SGP CART site.

ISCCP C2 data report the nonoverlapped (NOL) low, middle, and high TCAs, which can be used to estimate the low and middle ROL TCAs. Once we estimate the ISCCP ROL TCAs, we then compare them with the ECR and MPL–BLC estimates. Because of perspective, the satellite ROL equations differ from those derived for the ECR and MPL–BLC, that is, Eqs. (5) and (6). Analogous to Eq. (5), we have

$$\mathrm{TCA}_M^{\mathrm{ROL}} = \frac{\mathrm{TCA}_M^{\mathrm{NOL}}}{1 - \mathrm{TCA}_H^{\mathrm{NOL}}}, \tag{7}$$

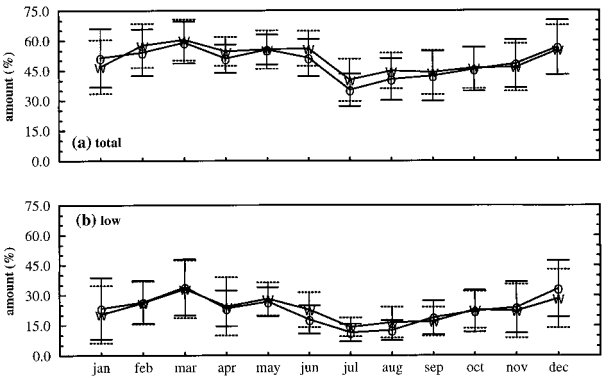

FIG. 1. Time average cloud amount (TCA) as a function of month for (a) total, and (b) low clouds. The curves labled ''w'' (dashed error bars) and ''o'' (solid error bars) represent climatologies for Wichita and Oklahoma City, respectively. The error bars represent a single standard deviation about the ECR mean.

where we have assumed $\mathrm{TCA}_H^{\mathrm{ROL}} = \mathrm{TCA}_H^{\mathrm{NOL}}$. The counterpart to Eq. (6) is

$$\mathrm{TCA}_L^{\mathrm{ROL}} = \frac{\mathrm{TCA}_L^{\mathrm{NOL}}}{1 - \mathrm{TCA}_H^{\mathrm{NOL}} - \mathrm{TCA}_M^{\mathrm{NOL}}}. \tag{8}$$

Rozendaal et al. (1995) apply Eq. (8) in their study of maritime stratiform clouds.

3. Results

There are a number of ways in which one can estimate the monthly or seasonal TCAs. In an attempt to mitigate any diurnal bias, we first average all observations for a particular reporting time of day and then use these to produce an average for the month or season. We apply this averaging procedure to both the ECR and MPL–BLC data. The ISCCP stage C2 data were processed similarly. The full temporal resolution of each dataset was used to compile the monthly statistics for total, low, middle, and high clouds. MPL–BLC and ISCCP data were sampled at the same temporal frequency as the ECR data (i.e., 0000, 0600, 1200, 1800 LST) for the diurnal/seasonal TCAs.

a. Platform intercomparison

We first compare the total and low ECR TCAs for the two stations used to produce the composite ECR climatology over the ARM CART. Figure 1 indicates that there is some spatial variability (and/or possible observer differences) associated with the TCAs at each location. The ''w'' (dashed error bars) and ''o'' (solid error bars) denote denote Wichita and Oklahoma City, respectively. The differences are generally small—especially when compared to the interannual variability. The differences in low TCA are small during spring and fall and reach a maximum during midwinter and summer (on the order of 5%). With the exception of winter, the

TABLE 2. Estimates of annual TCAs and interannual ECR standard deviations.

Type	ECR	Std dev	MPL–BLC	ISCCP
Total	50.0	2.7	52.8	49.2
Low	23.0	3.7	27.8	21.0
Mid	14.5	1.5	14.8	20.9
High	24.7	2.7	22.9	14.9

TABLE 4. Estimates of spring TCAs and interannual ECR standard deviations.

Type	ECR	Std dev	MPL–BLC	ISCCP
Total	56.0	5.7	60.3	55.5
Low	28.2	7.5	38.7	28.5
Mid	14.7	1.7	11.0	20.8
High	28.2	4.4	26.7	16.6

total TCAs are larger for Wichita but are also well within one standard deviation of their interannual variation.

Estimates of the annual and seasonal TCAs of total, low, mid, and high clouds for the three platforms and the ECR standard deviations are given in Tables 2–6. The MPL–BLC has the largest total annual TCA and its seasonal total TCA is larger than that of either the ECR or the ISCCP with the exception of summer. Similarly, the MPL–BLC also has the largest annual TCA for low clouds and is larger for all seasons except summer. With the exception of winter, the ECR produces the largest TCA for high clouds (nearly twice that of the ISCCP annual high cloud TCA). The ISCCP middle cloud TCAs (annual and seasonal) are greater than either the ECR or MPL–BLC TCAs except during the summer where the MPL–BLC middle cloud TCA is larger. There is good agreement between the ECR and ISCCP annual low cloud TCAs as well as between ECR and MPL–BLC annual high cloud TCAs (both within ≈2%). Annual estimates of the total cloud TCA indicate excellent agreement (<3%) for all three platforms with the largest (smallest) discrepancies in winter (spring). Note that for the ISCCP data, Eq. (4) is only approximately valid (within a few percent). ISCCP low, middle, and high cloud TCAs are determined from IR radiances only (both day and night). However, the total ISCCP TCA utilizes both VIS and IR radiances in the daytime, while nighttime values are adjusted by interpolating (between dusk and dawn) the differences between the daytime VIS–IR and IR only results.

We calculated the differences between the monthly means of the MPL–BLC and ECR total TCAs. The differences range from 18% (2.1 ECR standard deviations) in June to −14.6% (−1.2 ECR standard deviations) in December. We also estimated the ISCCP and ECR monthly total TCAs. To determine whether or not the differences between the ISCCP and ECR total TCA monthly means are statistically significant, we apply the small sample Student's t statistic (McClave and Dietrich 1982),

$$t = \frac{\overline{x}_1 - \overline{x}_2}{\left[s^2\left(\frac{1}{n_1} + \frac{1}{n_2}\right)\right]^{1/2}}, \tag{9}$$

where $\overline{x}_1$, n_1, and $\overline{x}_2$, n_2 are the monthly means and sample sizes for the ISCCP and ECR data, respectively, and the pooled sample variance s^2 is

$$s^2 = \frac{(n_1 - 1)s_1^2 + (n_2 - 1)s_2^2}{n_1 + n_2 - 2}, \tag{10}$$

where s_1^2 and s_2^2 are the ISCCP and ECR sample variances. We assumed that both ECR and ISCCP TCAs are approximately normally distributed, are independently sampled, possess equal population variances, and that the hypothesized difference between their means is zero. The rejection region (i.e., the region where the observed t values exceed those given by the probability density function of the t distribution) will be two-tailed (i.e., the rejection region can be either larger or smaller than some value) with the degrees of freedom equal to the sum of the degrees of freedom (16) for the two samples. Choosing a 95% confidence level, the rejection region is $t > 2.12$ or $t < -2.12$. The observed two-sample *t*-test statistic for each month indicates that *none* of the observed values of t fall in the rejection region—thus, we cannot conclude that there is a difference between any of the ISCCP and ECR monthly means. We do not perform a *t*-test using the MPL–BLC monthly means because they are composited from a sample size of one (i.e., zero degrees of freedom).

Figure 2 compares the monthly mean low, middle, high, and total TCAs from the ECR, ISCCP, and MPL–BLC data. In all figures, the solid, dashed, and dotted lines represent the TCAs from the ECR, ISCCP, and MPL–BLC datasets, respectively. The error bars, which indicate one standard deviation about the mean, depict the interannual variability of the monthly averages of the 10-yr ECR record.

ISCCP estimates of low cloud TCA (Fig. 2d) are

TABLE 3. Estimates of winter TCAs and interannual ECR standard deviations.

Type	ECR	Std dev	MPL–BLC	ISCCP
Total	53.7	9.2	60.4	51.1
Low	26.7	8.9	30.9	17.0
Mid	15.7	5.8	17.5	29.2
High	25.8	2.6	30.3	14.8

TABLE 5. Estimates of summer TCAs and interannual ECR standard deviations.

Type	ECR	Std dev	MPL–BLC	ISCCP
Total	44.5	5.5	39.6	42.3
Low	15.8	2.9	12.4	17.7
Mid	13.1	2.1	17.3	14.6
High	24.3	5.9	16.6	14.9

TABLE 6. Estimates of fall TCAs and interannual ECR standard deviations.

Type	ECR	Std dev	MPL–BLC	ISCCP
Total	45.5	7.3	51.2	48.0
Low	21.1	6.6	28.4	20.2
Mid	14.3	2.6	15.5	19.2
High	19.8	4.9	19.0	13.2

lower than those of both the MPL–BLC and ECR during winter. The ISCCP low cloud TCAs depend on the retrieved cloud-top pressures obtained from IR radiances only and may be underestimated because IR threshold techniques (used to identify pixels as clear or cloudy) have difficulty ''seeing'' low clouds when the radiance of the clouds is virtually indistinguishable from the cloud-free background (Rossow et al. 1985). This is especially problematic in the case of broken low cloud decks [e.g., stratocumulus (Sc), cumulus (Cu)] over cold surfaces.

In part due to obscuration by low clouds of higher clouds, observations taken by a human are typically best in the low levels while satellites might be expected to yield more accurate estimates of high cloud amount than of low or middle. ISCCP middle cloud TCAs differ significantly (especially winter) from those of the ECR in all but the late summer and early fall (July–September).

Despite the 10%–15% difference between the ISCCP and ECR high cloud TCA, the monthly variations are quite similar (Fig. 2b). The systematic overprediction of the ECR high cloud TCA may reflect the failure of the ROL—suggesting that there is some correlation between upper-level and lower-level clouds. It is also possible that the ISCCP data underreport (or misreport as a lower cloud deck) the high cloud TCA due to the optically thin nature of cirriform clouds (Jin et al. 1996). ISCCP has an improved cloud detection algorithm where the IR threshold has been reduced (over land) from 6 K to 4 K. This data is now available as the series D2 cloud product but was not used herein.

b. Monthly means

The annual cycle depicted by the total cloud amount (Fig. 2a) is determined primarily by the low cloud amount (Fig. 2d), which registers a March maximum and a July–August minimum. The high cloud amount annual cycle also closely matches the total cloud amount annual cycle (Fig. 2b). The summer minimum may come as somewhat of a surprise as Cu occurrence frequencies tend to be a maximum over the Great Plains during this time of year. However, as will be shown in the next section, the peak in summer Cu occurrence frequency is offset by a minimum in stratus (St) and Sc during the summer months. The summer total cloud TCA minimum is consistent with the seasonal variation in continental cloud cover observed in other cloud climatologies (e.g., van Loon 1972). Both the ECR and ISCCP datasets indicate a second peak in the total cloud amount in May and a relatively significant decrease (approximately 10%) in the total cloud amount from December to January.

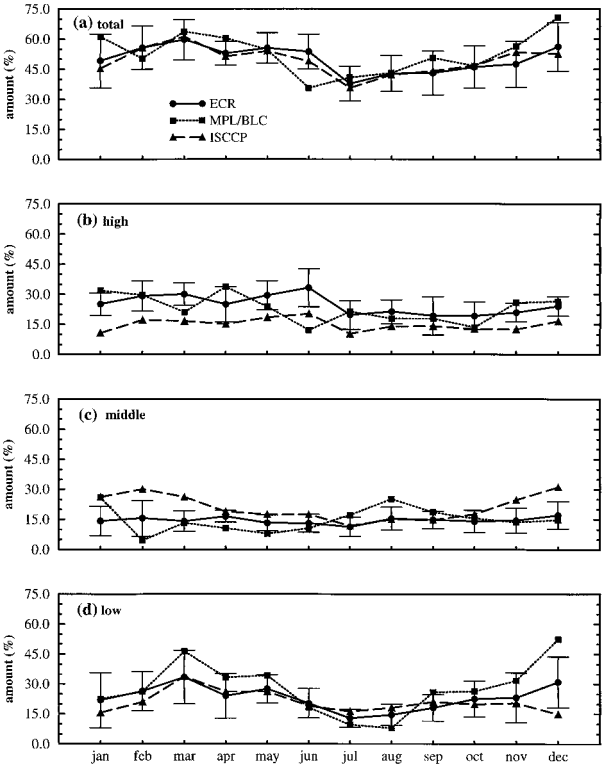

FIG. 2. ROL time average cloud amount (TCA) as a function of month for (a) total, (b) high, (c) mid, and (d) low clouds. The solid, dashed, and dotted lines denote the ECR, ISCCP, and MPL–BLC TCAs, respectively.

c. Diurnal cycles by season

Diurnal statistics (i.e., cloud amount vs time of day) from all three sources are presented by season for total, low, middle, and high clouds (Figs. 3–6). The error bars represent the ECR interannual variability (i.e., one standard deviation) of the seasonal means at 0000, 0600, 1200, and 1800 LST, respectively. With the exception of 0600 LST summer, the seasonal ISCCP total TCAs lie within a single standard deviation of the ECR total TCAs. Diurnal variation in the total TCA is low for all three platforms except for summer MPL–BLC, which indicates a 0600 LST maximum and 1200 LST minimum (Fig. 3c). Comparison of the total TCAs for the three platforms indicates that the ECR and ISCCP are in better agreement with one another than either are with the MPL–BLC. The low cloud ECR standard deviations are smallest in the summer (Fig. 4c). (We restrict the discussion of interannual ECR standard deviations to a seasonal comparison as the nighttime interannual vari-

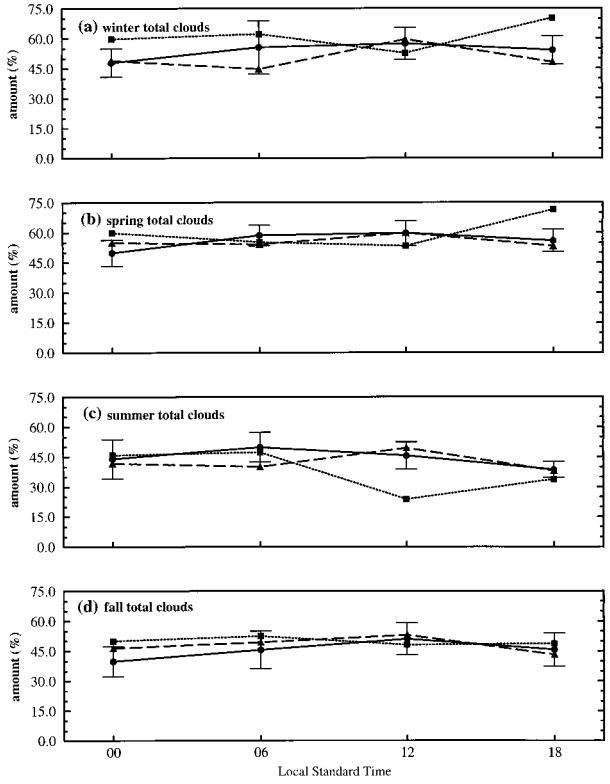

FIG. 3. Total cloud TCA as a function of hour for (a) winter, (b) spring, (c) summer, and (d) fall.

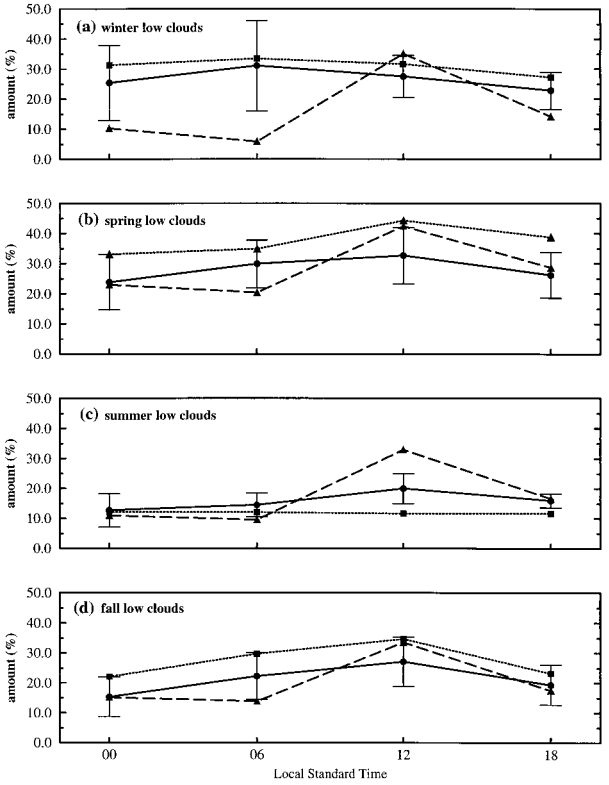

FIG. 4. Same as in Fig. 3 except for low clouds.

ances are generally larger than their daytime counterparts due to the restrictive sampling of the nocturnal data.) The diurnal cycle for the ECR and MPL–BLC low cloud TCAs is most pronounced during the fall and smallest during the summer. With the exception of winter, where the maximum occurs at 0600 LST, the diurnal low cloud peak occurs at 1200 LST. The nocturnal estimates of low cloud amount from the ISCCP dataset are lower than those from either the ECR or MPL–BLC. The steep increase in the ISCCP low cloud TCA between 0600 LST and 1200 LST is likely related to the IR threshold technique, which tends to miss nocturnal low-level clouds, especially during the winter (Fig. 4a) when temperature inversions make the detection of Cu and Sc extremely difficult (Rossow and Garder 1993). In summer, the nocturnal ISCCP low cloud TCA is comparable to that of the MPL–BLC and ECR (Fig. 4c). Figure 5 indicates a middle cloud maximum at 0600 LST for both ISCCP and ECR TCAs (except during the winter for ISCCP) while the MPL–BLC TCA exhibits a 0600 LST maximum in summer only. The diurnal cycle is most pronounced for the summer MPL–BLC TCA while the agreement between the summer ECR and ISCCP TCAs is quite good. As with low clouds, the interannual middle cloud variability is largest during the winter. Both spring and summer exhibit small in-

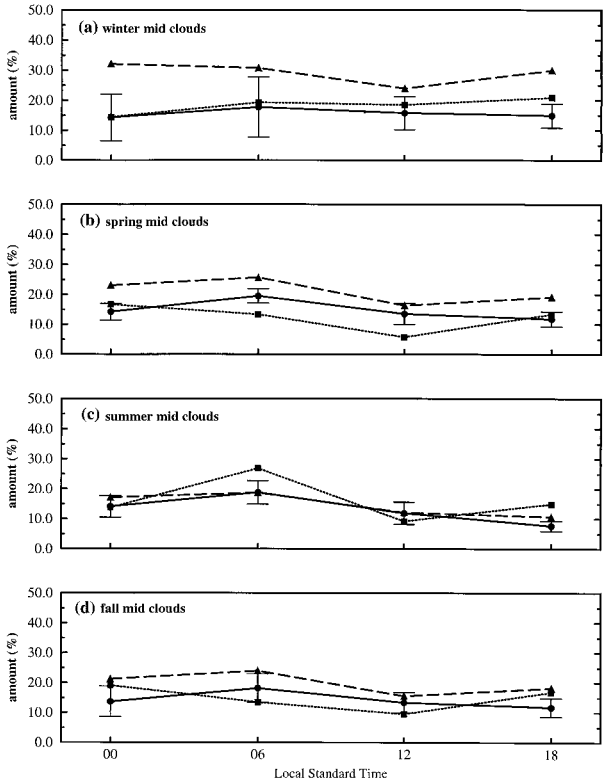

FIG. 5. Same as in Fig. 3 except TCA^{ROL} for middle clouds.

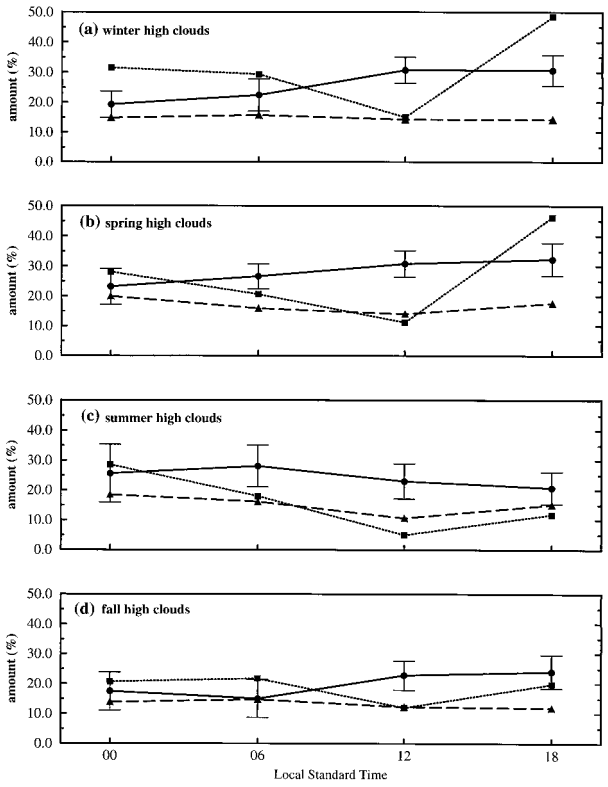

FIG. 6. Same as in Fig. 3 except TCA^{ROL} for high clouds.

terannual variations with a summer minimum at 1800 LST.

The large increase in the MPL–BLC high TCA between 1200 and 1800 LST, in particular in winter and spring (Fig. 6), is somewhat suspicious. Background noise, which is a limiting factor in daylight lidar measurements, requires a signal average over several minutes to detect cirrus (Spinhirne 1993). Consequently, the one minute temporal resolution of the MPL–BLC data used herein may be inadequate. In the presence of solar noise, the cloud mask algorithm (Clothiaux et al. 1998) may identify some noncloudy scenes as cloudy. However, one might expect to find this problematic in the summer rather than winter and spring as indicated in Fig. 6. In contrast to the the MPL–BLC high cloud TCA, diurnal variations in the ISCCP high cloud TCA are small. The high cloud interannual variability is comparable for all seasons and, in general, does not show a seasonal bias.

d. Individual cloud types

The diurnal cycle by season of the TCA for individual WMO cloud types are presented in this section for the ECR data only. Although the TCA for individual cloud types exists for the ISCCP dataset, they are for daytime conditions only and correspondence between ISCCP and WMO cloud types is difficult to assign and thus are not included herein. The cloud types are defined using the WMO codes for low (C_L), middle (C_M), and high (C_H) clouds listed in Table 7. Although available in the ECR, Fog ($C_L = 11$) TCA are not reported herein. Note that WMO codes greater than nine are not standard but have been added to account for the special cloud types, nimbostratus (Ns) and obscured cumulonimbus (Cb). As with the estimates of total, low, middle, and high cloud TCAs, we calculate the TCAs for the individual cloud types using only those observations where the nocturnal illuminance criterion is satisfied.

TABLE 7. WMO cloud codes.

Low	C_L	Middle	C_M	High	C_H
Cu	1, 2	Ac	3, 4, 5, 6, 7, 8, 9	Ci	1, 2, 3, 4, 9
Sc	4, 5, 8	As	1, 2	Cs	5, 6, 7, 8
St	6, 7	Ns	10, 11, 12		
Cb	3, 9, 10				

To determine the TCAs for the individual middle and high cloud types (C_j = Ac, As, Ci, and Cs; altocumulus, altostratus, cirrus, and cirrostratus, respectively), we calculate the underlying TCA associated with each cloud type TCA_L^{NOL} (C_j), and apply

$$\mathrm{TCA}(C_j) = \frac{\mathrm{TCA}^{\mathrm{NOL}}(C_j)}{1 - \mathrm{TCA}_L^{\mathrm{NOL}}(C_j)}, \qquad (11)$$

where $TCA^{NOL}(C_j)$ is the NOL TCA for the cloud type C_j. Note that the $TCA_L^{NOL}(C_j)$ is not strictly a TCA by definition as it represents an average low-level cloud amount calculated from a subset of observations. It would be more appropriate to refer to this quantity as the TCA-when-present, since it is a time average of the underlying cloud amount in the presence of a particular upper-level cloud type.

Although expressed in a form similar to the ROL given by Eq. (5), Eq. (11) is *not* a true ROL for individual cloud types because $TCA^{NOL}(C_j) + TCA_L^{NOL}(C_j) \neq TCA_T$. As the number of obscured observations increases, the $TCA(C_j)$ approaches zero. Because obscured observations may contribute to an underprediction of actual upper level TCAs for individual cloud types, we do not use them when calculating upper-level NOL TCAs. Middle and high cloud ROL TCAs [using Eqs. (5) and (6)] are not affected by the number of obscured observations because the cloud amount for the underlying layer(s) is (are) taken as the actual low TCA rather than the TCA-when-present for a given cloud type. With the exception of As–Ac, Hahn et al. assume that the AWP and COF of upper-level clouds are the same when they cannot be seen as when they can. However, in order to account for nonrandom overlap effects, they adjust the COF for As–Ac by assigning a mean frequency (computed from As–Ac with low cloud amounts ranging from 3 to 7 oktas) when the low levels are overcast. We do not attempt to apply this type of correction to our estimates of $TCA(C_j)$. Consequently,

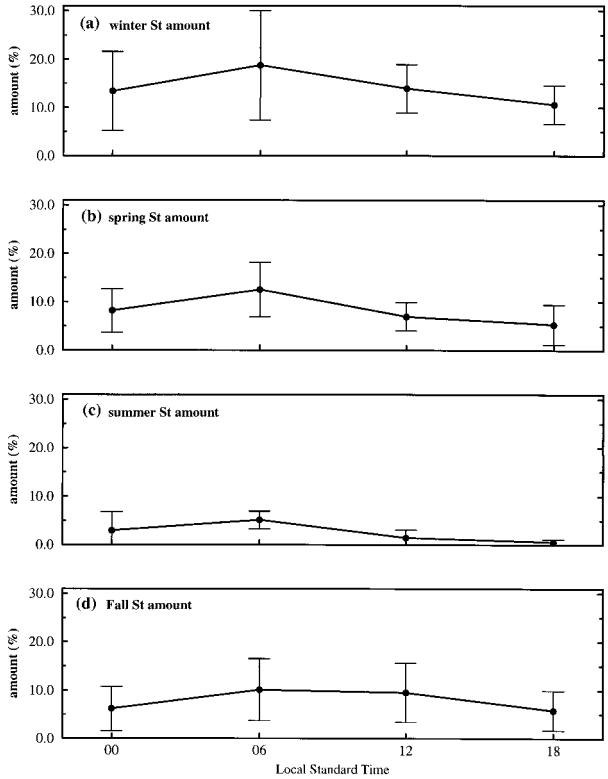

FIG. 7. Same as Fig. 3 except for stratus.

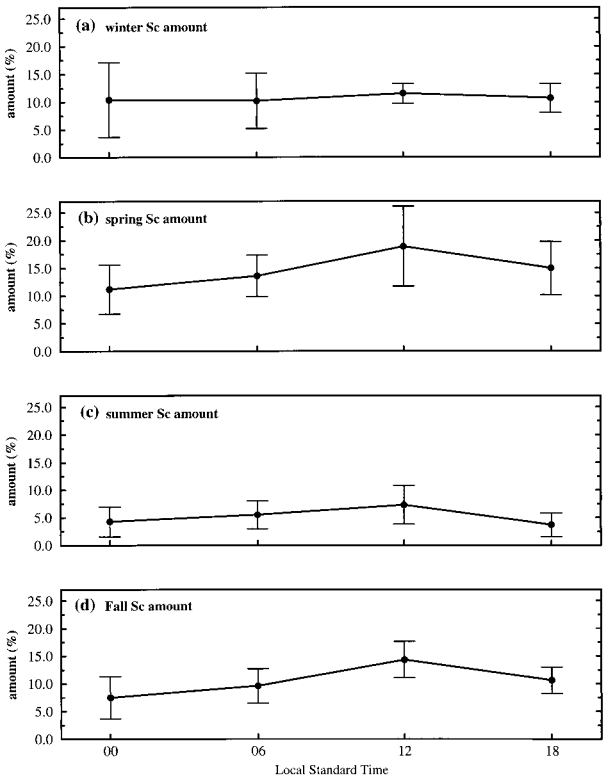

FIG. 8. Same as Fig. 3 except for stratocumulus.

our upper-level cloud amount estimates will also differ from those of Hahn et al. depending on the relative number of obscured-to-visible observations, and the adjusted COF in addition to the fundamental differences in the two methodologies (see section 2a).

To gauge the applicability of the random overlap assumption [Eq. (1)], we calculate the COF as a function of low cloud amount (figure not shown). We see increasing frequencies for increasing low cloud amount (i.e., random overlap is not valid) for As, a finding that indeed suggests that there may be more As than reported in the paper. Trends in other upper-level clouds are not conclusive. Hahn et al. also relax the ROL for Ns (for which they assume minimum overlap), and the COF for Ci are restricted to low-level cloud amount less than 7 oktas.

We follow Hahn et al. and assign, when Ns are present, the total cloud cover (N) as the Ns amount (i.e., minimum overlap). When calculating the total number of observations, we also omit those reports where the cloud type is reported present but the amount is missing. Similar to the impact of obscured observations, actual NOL cloud amounts will differ if the NOL amounts for the times they are not available differ substantially from the NOL amounts for the times when they are available. The impact will depend on the ratio of the unavailable-to-available reports when the cloud type is reported present. We calculate this ratio for each middle- and upper-level cloud type. These ratios are largest for Cid (0.48) and Ac (0.26) and suggest, especially for these two cloud types, the TCAs presented herein may not be representative of their *actual* values.

1) LOW CLOUDS

Figure 7 shows that St are most prevalent during the winter and occur infrequently during the summer. There are significant seasonal differences in the amplitude of the diurnal cycle, with the most (least) pronounced diurnal cycle occurring during the winter (summer). The diurnal variations are similar for all seasons with a 0600 LST diurnal maximum and 1800 LST minimum. Winter St show considerable interannual variability (Fig. 7a) especially at 0600 LST. In contrast, summer St show little in the way of interannual variance (Fig. 7c). Ratios of bad-to-fair weather St, TCA($C_L = 7$)/TCA($C_L = 6$), range from 0.2 to 1.0 with a spring maximum at 1800 LST (the large winter St TCAs are associated primarily with fair weather). Sc TCA peaks in the spring (Fig. 8b) and has a summer minimum (Fig. 8c). The diurnal cycle of Sc is most pronounced during spring with a maximum at noon (primarily associated with $C_L = 5$). The same pattern is observed for other seasons but is reduced in amplitude. The interannual variability is largest for spring Sc. The summer and fall Sc standard deviations are comparable in magnitude. The diurnal Cu

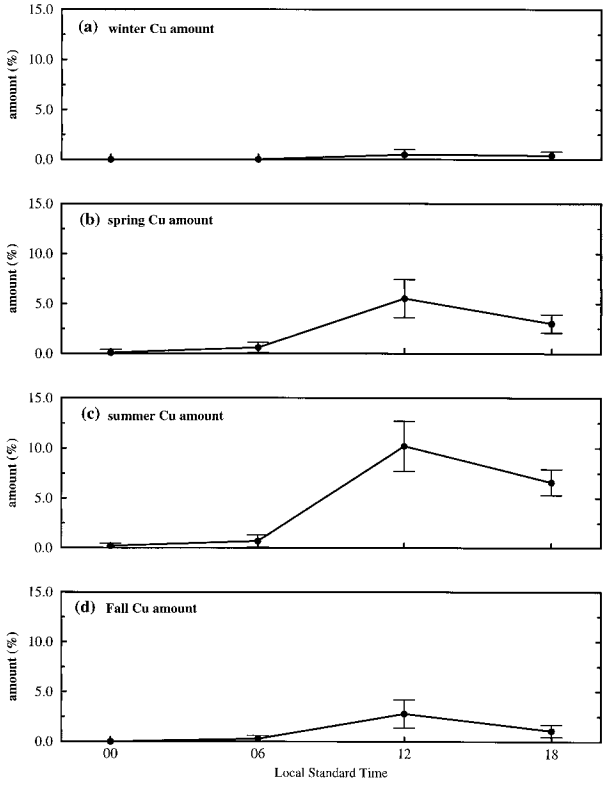

FIG. 9. Same as Fig. 3 except for cumulus.

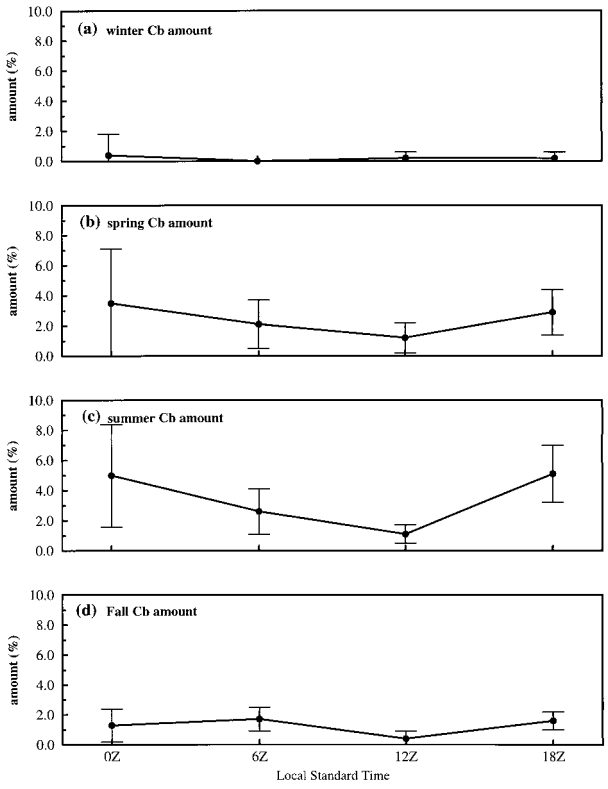

FIG. 10. Same as Fig. 3 except for cumulonimbus.

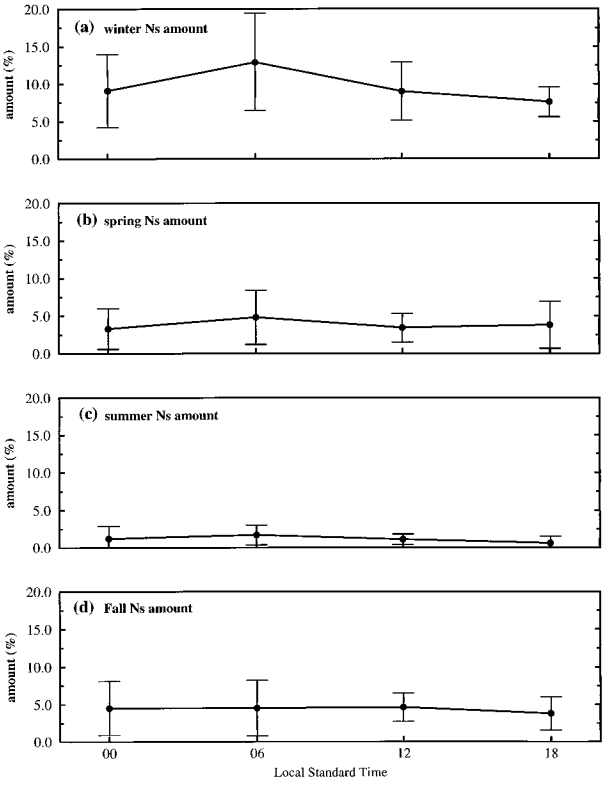

FIG. 11. Minimum overlap TCA for nimbostratus as a function of hour for (a) winter, (b) spring, (c) summer, and (d) fall.

cycle, as one might expect, exhibits large (small) summer (winter) fluctuations and has a noon maximum in all seasons (Fig. 9). Diurnal variations in Cu TCA range from less than 1% in the winter to as large as 10% in the summer while the interannual variability is greatest (smallest) during the summer (winter).

The ECR dataset assumes Cb to be a low cloud type because its base generally occurs in the low levels. Figure 10 indicates that Cb are observed with greater frequency during the summer than spring despite the spring peak in Oklahoma severe weather (Johnson and Duchon 1995). Similar to Cu, the diurnal Cb cycle is most pronounced during the summer with a weak signal in the winter. The diurnal minimum occurs at noon (with the exception of winter) while summer experiences an early evening peak (18 LST) and in winter–spring, a midnight maximum.

2) MIDDLE CLOUDS

The ECR has a special provision for Nimbostratus in which codes C_M = /, 2, or 7 are taken as Ns (and extended to C_M = 10, 11, 12 in the ECR) if there is precipitation and a certain combination of low cloud types. Figure 11 indicates that Ns are most common in winter and occur with the least frequency during the summer. The diurnal cycles are weak (on the order of

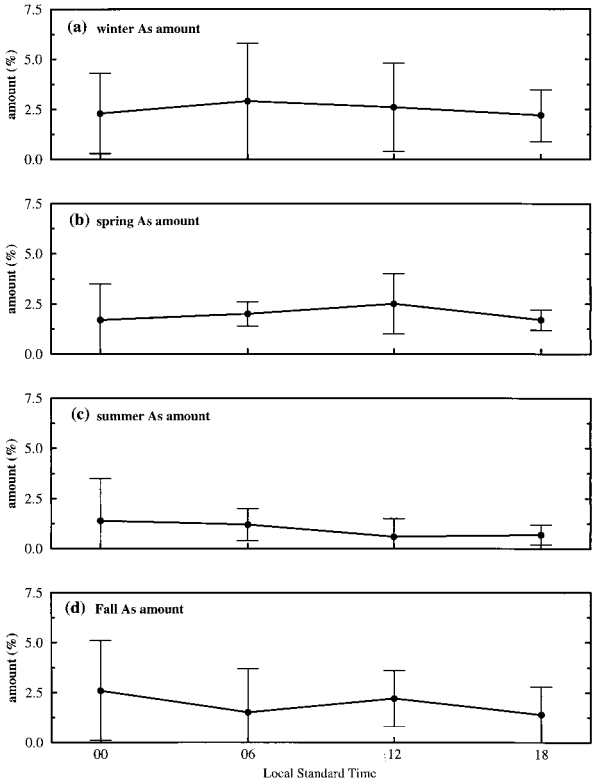

FIG. 12. Same as Fig. 3 except for altostratus.

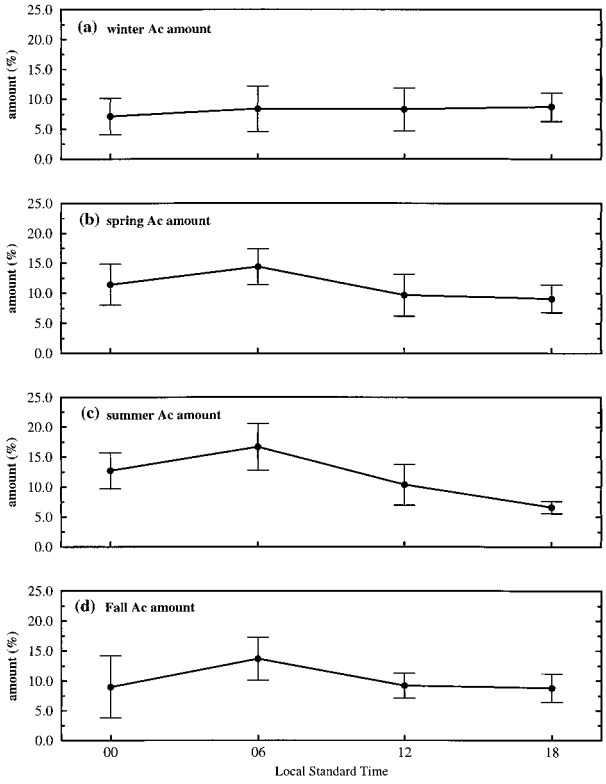

FIG. 13. Same as Fig. 3 except for altocumulus.

a couple of percent), with the exception of winter where the diurnal variations approach 10%. Altostratus TCA shows little seasonal variation and has a weak diurnal cycle (Fig. 12). Altostratus exhibits its largest interannual variance during the winter.

Because Ac are relatively common (compare Figs. 12 and 13 where Ac TCAs are as much as 10 times larger than As TCAs), yet little studied, their impact on the global radiation budget and climate are of particular interest. They have a primarily liquid water constitution and a similarity to Sc in that they are often convectively destabilized by their radiative heating profiles (Heymsfield et al. 1991; Liu and Krueger 1997). Herein, the Ac category includes all but two of the C_M codes.

Although Ac TCA is largest during the summer and the peak in its diurnal cycle appears to follow (i.e., lags by 6 h) that of the Cb TCA, the Ac annual cycle is mainly determined by the $C_M = 7$ cloud type (noninvasive, translucent or opaque, multilayer Ac or a combination of Ac, As, and Ns) while all other types combined, including $C_M = 6$ (Ac from spreading Cu or Cb), contribute little to the TCA. The seasonal cycle of Ac TCA has a minimum in winter. The diurnal Ac cycle exhibits a 0600 LST maximum in all seasons except winter. Its diurnal cycle is most pronounced in the summer. That the diurnal signal is strongest during the summer (note the ~10% decrease in Ac TCA between 0600 LST and 1800 LST) suggests that the daytime shortwave radiation effectively counters the impact of the IR cloud-top cooling thereby reducing the circulations responsible for the maintenance of the Ac layer. This finding agrees with the numerical simulations of Liu and Krueger (1997), which show that radiative heating in an Ac layer during the day stabilizes the cloud layer, weakens the circulations that drive and maintain the Ac, and thus reduces or dissipates the Ac. The interannual variability is ostensibly independent of season with the largest standard deviation (>5%) at 0000 LST during the fall. It is also possible that the day/night sampling bias may be responsible for the large diurnal signal in summertime Ac. We examined the ratio of the number of observations that satisfy the illuminance criteria to the total number of observations and found that the summer has nearly four times the number of ''light'' observations than does the winter. However, if one compares the fall 0600 LST Ac TCA with that of spring (which has 22% more light observations than fall), we see that the *increase* in fall Ac TCA between 0000 and 0600 LST is actually greater than it is for spring (note that the number of illuminated 0000 LST observations are roughly independent of season). This is not consistent with the hypothesis that the 0600 LST peak is associated with the ''enhancement of the nighttime–dawn Ac TCA relative to winter.'' If this were the case then one would expect the spring increase in Ac TCA between the hours of 0000 and 0600 LST to be larger than fall. Also note

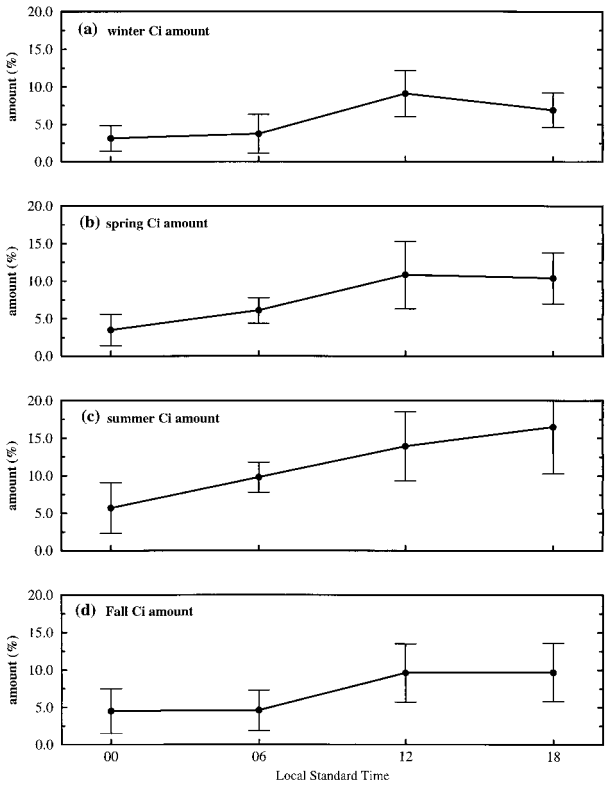

FIG. 14. Same as Fig. 3 except for cirrus.

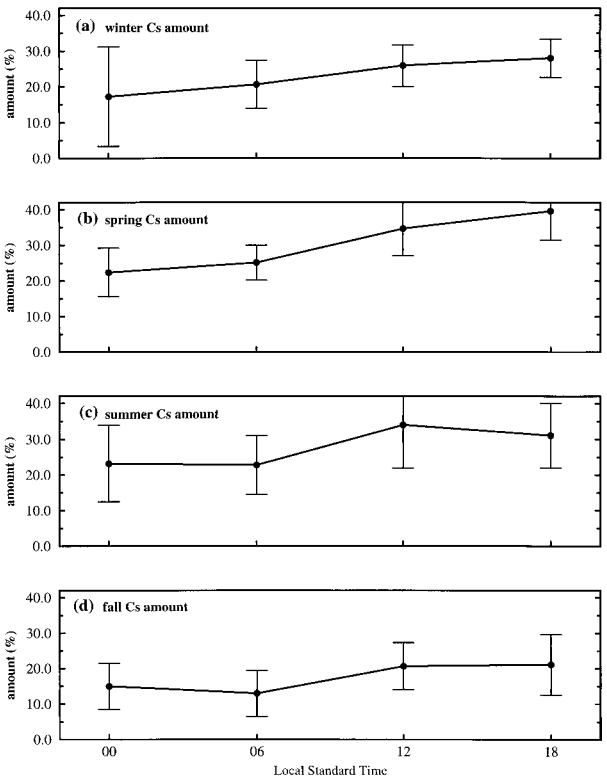

FIG. 15. Same as Fig. 3 except for cirrostratus.

that winter 0000 LST Ac TCA is small (compared with other seasons) and there is quite a bit of seasonal variability (on the order of what is seen at 0600 LST), even though the number of observations that satisfy the illuminance criteria at 0000 LST do not vary much from season-to-season (these range from 0.26 to 0.33).

3) HIGH CLOUDS

The seasonal variations in Ci and Cs TCA are slight with the smallest Ci TCAs occurring in spring and winter (0000 LST) and smallest Cs TCAs occurring during the fall (Figs. 14 and 15, respectively). Summer registers larger Ci TCAs. This could be related to the summer peak in Cb frequency. However, it should be pointed out that the contribution of $C_H = 3$ (i.e., thunderstorm anvil) to the Ci TCA is quite small. Note that the Ci TCA is dominated by $C_H = 1$ (noninvasive Ci in the form of strands). Additionally, the diurnal cycle of Cs TCAs do not resemble those of Ci as one might expect if they were formed from deep convection. The Cs TCAs are slightly larger in spring (than winter or summer) and are smallest in fall. The diurnal pattern of the ECR TCAs for Ci and Cs are quite similar—varying from a nocturnal minimum to a midday or late afternoon maximum. Nocturnal Ci TCAs are on the order of 5%–10% less than the daytime values. This may or may not represent a real difference and the illuminance threshold should reduce problems associated with the lack of visibility. Daytime interannual fluctuations in Ci and Cs TCAs are generally largest during the summer (Figs. 15c and 15d).

4. Summary

Estimates of mean monthly, seasonal, and annual total low, middle, and high cloud amounts were calculated using three disparate sources over the SGP ARM CART site in north-central Oklahoma. The ECR data were composited from a 10-yr record of the synoptic weather reports of two stations: Oklahoma City, Oklahoma, and Wichita, Kansas. The ISCCP data, selected from a grid cell over the ARM SGP CART, covered an 8-yr period. The MPL–BLC data, which were collected directly at the CART facility, span a 1-yr period.

Caution should be exercised when comparing climatologies derived from different sources. Satellite data represent a larger field-of-view than that of a human observer while the MPL and BLC sample only a small segment of sky directly overhead but do so continuously. Using the ROL, which assumes that the cloud layers are independent of one another, we attempt to represent cloud amount in terms of the actual (i.e., the cloud amount present whether visible or not) amount rather than the nonobscured amounts. The accuracy of the ROL will likely depend on large-scale weather pat-

terns but its performance may also be influenced by local circulations and topography, which impact cloud morphology.

As a potential contributor to a CART climatology, the millimeter-wavelength cloud radar (MMCR; Moran et al. 1998) has the capability to provide cloud information through the entire troposphere and thus can be used to test the various cloud overlap assumptions. However, the operation of the MMCR has been of too short duration, as of yet, to contribute to a climatology. Highlights of the intercomparison include:

- The annual cycle for all three datasets compare favorably for the total cloud TCA. The agreement is especially good between the ISCCP and ECR datasets and *t*-scores indicate that the differences between the two are not statistically significant.
- Relatively good agreement in the annual cycle of the monthly low cloud TCA for the ECR and MPL–BLC data.
- ECR monthly mean high cloud TCA estimates are typically 5%–10% greater than the ISCCP high cloud TCAs (Jin et al. 1996).
- Winter ISCCP low cloud amount estimates are generally 5%–10% less than those calculated from the ECR and MPL–BLC data (Rossow and Garder 1993).
- The observed diurnal variations of Ac support cloud-resolving model results.
- There is a possible high cloud lidar detection problem resulting from solar noise.

Otherwise, expected diurnal and seasonal variations in low, middle, and high clouds are evident. Low cloud coverage is at a minimum during summer. The peak in summer Cu TCA are offset by a minimum in both Sc and St TCA. The Cu diurnal maximum (minimum) TCA occurs at 1200 LST (0000 LST) with summer (winter) experiencing the largest (smallest) diurnal variation. The St are most common in winter while Sc are observed more frequently during spring. The St exhibits a diurnal maximum at 0600 LST and Sc at 1200 LST. Perhaps somewhat surprising, Cb are most commonly observed during the summer rather than spring. The diurnal maximum occurs at 0000 LST during the winter and spring, but shifts to 1800 LST during the summer. The Ac are more common than Ns for all seasons with the exception of winter Ns. The interannual variability is large for nighttime winter Ns and As. Winter and spring Cs display similar diurnal cycles with increasing TCAs from 0000 LST to 1800 LST. The Ci nocturnal TCAs are less than the daytime values. Both Ci and Cs TCAs show relatively little seasonal variation.

Although direct comparison of the three platforms is quite difficult, estimates of the total cloud amount appear to be robust—a finding that is supported by the *t*-test, which indicates no significant difference between any of the ISCCP and ECR monthly means. Low cloud TCAs for both the MPL–BLC and ECR, which do not invoke the ROL assumption, are likely somewhat reliable as indicated by their similar annual and diurnal cycles. In terms of individual observing systems, the diurnal and annual trends of the ECR low TCA as well as for Sc, St, Cu, and Cb are consistent with midlatitude low cloud climatologies. Even though they are unobscured, ISCCP high cloud amounts are likely underestimated, in part due to a relatively conservative IR threshold used to differentiate between cloudy and clear skies. The degree to which the IR threshold impacts the climatology will be examined in a future investigation using the series D2 dataset. The D2 data relax the IR threshold (i.e., the minimum difference, between the background IR radiance and observed radiance, required for cloud detection) from 6 to 4 K. Comparisons of the various obscured cloud types indicates that only Cid and Cic exhibit tendencies suggestive of true random overlap.

The local climatology presented herein was designed to provide an estimate of cloud type and amount over the ARM CART site while evaluating and investigating the differences in three specific observing platforms. This study represents a first attempt to produce a CART site climatology. Ideally, these statistics can be used to test existing cloud parameterizations. Additional climatologies can also be constructed from the MPL, BLC, MMCR, and whole sky imager data as extended time observations become available. Because the ARM focus falls primarily on clouds and their impact on the radiation budget detailed cloud observations are essential to the programmatic objectives. Ideally, these observations can be used to verify existing cloud parameterizations as well as develop new (and improved) schemes for GCMs.

Acknowledgments. This research was supported by the Environmental Science Division, DOE, under Grants DE-FG03-94ER61769 and DE-FG03-94ER61747. The ISCCP data were obtained from the NASA Langley Research Center EOSDIS Distributed Active Archive Center. The ECR data were provided by Joel Norris of the Climate and Global Dynamics Division at the National Center for Atmospheric Research.

REFERENCES

Allis, R. J., and S. Raman, 1995: Diurnal variations in cloud frequency of the Gulf Stream locale. *J. Appl. Meteor.,* **34,** 1578–1594.

Clothiaux, E. E., G. G. Mace, T. P. Ackerman, T. J. Kane, J. D. Spinhirne, and V. S. Scott, 1998: An automated algorithm for detection of hydrometeor returns in micropulse lidar data. *J. Atmos. Oceanic Technol.,* **15,** 1035–1042.

Hahn, C. J., S. G. Warren, and J. London, 1994: Edited synoptic cloud reports from ships and land stations over the globe, 1982–1991. Tech. Rep. NDP-026B, 47 pp. [Available from Carbon Dioxide Information Analysis Center, Oak Ridge National Laboratory, Oak Ridge, TN 37831-6335.]

Heymsfield, J. A., L. M. Miloshevich, A. Slingo, K. Sassen, and D. O'C. Starr, 1991: An observational and theoretical study of highly supercooled altocumulus. *J. Atmos. Sci.,* **48,** 923–945.

Hughes, N. A., 1984: Global cloud climatologies: A historical review. *J. Appl. Climatol.,* **23,** 724–751.

Jin, Y., W. B. Rossow, and D. P. Wylie, 1996: Comparison of the climatologies of high-level clouds from HIRS and ISCCP. *J. Climate*, **9,** 2850–2879.

Johnson, H. L., and C. E. Duchon, 1995: *Atlas of Oklahoma Climate.* University of Oklahoma Press, 152 pp.

Liu, S., and S. K. Krueger, 1997: Effects of radiation in simulated altocumulus cloud layers. Preprints, *Ninth Conf. on Atmospheric Radiation*, Long Beach, CA, Amer. Meteor. Soc., 330–334.

McClave, J. T., and F. H. Dietrich, 1982: *Statistics.* Dellen Publishing, 766 pp.

Moran, K. P., E. M., Brooks, M. J. Post, R. A. Kropfli, D. C. Welsh, and K. B. Widener, 1998: An unattended cloud-profiling radar for use in climate research. *Bull. Amer. Meteor. Soc.*, **79,** 443–455.

Newell, R. G., J. W. Kidson, D. G. Vincent, and G. J. Boer, 1970: *The General Circulation of the Tropical Atmosphere and Interactions with Extratropical Latitudes.* Vols. 1 and 2. The MIT Press, 651 pp.

Rossow, W. B., and A. W. Walker, 1991: International Satellite Cloud Climatology Project (ISCCP) documentation of cloud data (Stage C2). WMO Tech. Doc. 266, World Meteorological Organization, 78 pp and 3 appendixes.

——, and R. A. Schiffer, 1991: ISCCP cloud data products. *Bull. Amer. Meteor. Soc.*, **72,** 2–20.

——, and L. C. Garder, 1993: Validation of ISCCP cloud detections. *J. Climate*, **6,** 2370–2392.

——, and Coauthors, 1985: ISCCP Cloud Algorithm Intercomparison. *J. Climate Appl. Meteor.*, **24,** 877–903.

Rozendaal, M. A., C. B. Leovy, and S. A. Klein, 1995: An observational study of diurnal variations of marine stratiform cloud. *J. Climate*, **8,** 1795–1809.

Short, D. A., and J. M. Wallace, 1980: Satellite-inferred morning-to-evening cloudiness changes. *Mon. Wea. Rev.*, **108,** 1160–1169.

Spinhirne, J. D., 1993: Micro pulse lidar. *IEEE Trans. Geosci. Remote Sens.*, **31,** 48–55.

Stokes, G. M., and S. E. Schwartz, 1994: The Atmospheric Radiation Measurement (ARM) Program: Programmatic background and design of the Cloud and Radiation Test Bed. *Bull. Amer. Meteor. Soc.*, **75,** 1201–1221.

Tian, L., and J. A. Curry, 1989: Cloud overlap statistics. *J. Geophys. Res.*, **94,** 9925–9935.

van Loon, H., 1972: Cloudiness and precipitation in the Southern Hemisphere. *Meteorology of the Southern Hemisphere, Meteor. Monogr.*, No. 13, Amer. Meteor. Soc., 101–104.

Warren, S. G., C. J. Hahn, J. London, R. M. Chervin, and R. L. Jenne, 1988: Global distribution of total cloud cover and cloud type amounts over land. NCAR Tech. Note TN-273+STR, Boulder, CO, 29 pp. and 200 maps.

World Meteorological Organization, 1988: Manual on codes. Vol. 1. WMO Publ. No. 306, WMO, Geneva.